Investigating the Impact of Drug Induced Pupil Dilation on Automated Iris Recognition

Inmaculada Tomeo-Reyes[1], Arun Ross[2], Vinod Chandran[1]

[1] Queensland University of Technology, Brisbane, QLD 4000, Australia

{inma.tomeoreyes, v.chandran}@qut.edu.au

[2] Michigan State University, East Lansing, MI 48824, USA

rossarun@msu.edu

Abstract

Recent research has demonstrated the negative impact of pupil dilation on iris recognition performance. Apart from light intensity changes, several factors such as alcohol, drugs, age, disease and psychology, are known to affect the size of the pupil. This work (1) analyzes the impact of drugs on pupil dilation, (2) proposes the use of a biomechanical nonlinear iris normalization scheme along with key point-based feature matching for mitigating the impact of drug-induced pupil dilation on iris recognition, and (3) investigates differences between drug-induced and light-induced pupil dilation on iris recognition performance. Experimental results indicate performance improvement when nonlinear normalization is used along with key point-based feature encoding for matching iris images with large differences in pupil size.

1. Introduction

The iris is a thin ring-shaped mobile diaphragm that separates the anterior and posterior chambers of the eye. The central aperture of the iris is the pupil. It is protected by the cornea, a transparent structure that, together with the lens, provides the refractive power of the eye. The iris has two main layers. The posterior layer is the pigmented epithelium, which consists of heavily pigmented epithelial cells that make it impenetrable by light. The anterior layer or stroma consists of cells and fibers that create a meshwork of connective tissue in which the blood vessels and nerves are integrated. The stroma is separated into the pupillary and ciliary zones, which are divided by a circular zigzag ridgeline known as the collarette. The pupillary zone shows small connecting crests and a pigment frill where the posterior layer's heavily pigmented tissue shows at the boundary. The ciliary zone contains interlacing ridges resulting from stromal support, contraction furrows that vary with the state of the pupil, irregular atrophies of the border layer called crypts, and freckles or moles, which are local collections of pigment cells. The stroma connects to two sets of involuntary muscles, the sphincter pupillae and the dilator pupillae. As per Tubbs *et al*. [23]: "The parasympathetic-innervated sphincter muscle fibers are circumferentially arranged to constrict pupil size, whereas the sympathetic-innervated dilator muscle fibers are radially arranged to widen pupil size" (see Figure 1).

Non-elastic deformation of the iris tissue occurs as a pupillary response to different stimuli, and the visible features of the stroma change perceptibly, as seen in Figure 2. Apart from variations in ambient light, changes in pupil size can also occur due to alcohol [2], drugs [7, 19, 21], diseases [3], or psychological factors [9, 11]. Furthermore, pupil size is affected by age [26], with smaller pupils being predominant among the elderly population.

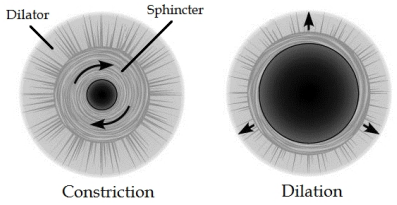

Figure 1: Pupillary light reflex (PLR). Parasympathetic stimulation causes sphincter muscle to contract for pupil constriction (left) and sympathetic stimulation causes dilator muscle to contract for pupil dilation (right).

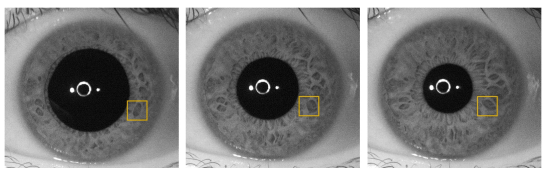

Figure 2: Effect of changes in pupil size on the iris texture. The highlighted box shows an example of changes on the visible features of the stroma, such as crypts and the collarette, when the pupil dilates or constricts.

Table 1: Existing research that systematically study the impact of pupil size on iris recognition performance.

Authors	Factor	Comments	Database (iris classes, images)
Arora *et al*. [2]	Alcohol	Score level analysis when matching iris images before and after alcohol consumption	IIITD-IUAI (110, 440)
Tomeo-Reyes *et al*. [21]	Drugs Light	Bit level analysis of the consistency of different iris regions using mean normalized bit error	In-house database (118, 448)
Dhir *et al*. [7]	Drugs	Score level analysis of the effect of cataract surgery and drug-induced pupil dilation on iris recognition	In-house database (15, 45)
Hollingsworth *et al*. [12]	Light	Score level analysis when matching images under varying degrees of light-induced dilation	In-house database (36, 1263)
Wei *et al*. [25]	Light	Deformation correction by using a Gaussian function to model the deviation from the linear stretch	CASIAv3-Lamp [1] (400,6000), in-house database (30, 1800)
Thornton *et al*. [20]	Light	Distortion-tolerant similarity metric defined from a MAP estimate of the parameters of the deformation	CASIAv1 [1] (108, 756), in-house database (101,$\sim$2500)
Yuan and Shi [28]	Light	Nonlinear normalization based on Wyatt's model [27]	SJTU-IDBv2 (200, 1000)
Tomeo-Reyes *et al*. [22]	Light	Nonlinear normalization based on biomechanical model [4]	WVU-PLS [5] (48, 1010)

The use of iris texture for automated recognition of individuals is commonly referred to as iris recognition. Changes in pupil size between two iris images of the same individual can affect iris recognition performance. This has been demonstrated in the case of changes induced by alcohol [2], drugs [7, 21] and light intensity [12]. While the effect of ageing on iris recognition has been investigated [8, 10], there is no direct evidence in the biometric literature thus far which indicates that changes in recognition performance are induced by changes in pupil size due to ageing.

1.1. Related work

The impact of changes in pupil size on iris recognition performance was first reported by Ma *et al*. [14], who recorded a number of false non-matches due to pupil dilation. This highlighted the need to further explore the effects of pupil dilation on iris recognition and, since then, extensive analysis has been carried out to demonstrate the impact of varying degrees of pupil dilation on iris recognition performance (see Table 1). However, only a few solutions have been developed to counteract this impact on iris recognition performance. For example, Thornton *et al*. [20] and Wei *et al*. [25] proposed learning-based approaches to address the problem. Although both approaches improve iris recognition performance, their potential is limited by the fact that they are dependent on the particular dataset used for parameter estimation.

Given the nonlinear nature of the iris deformation when the pupil dilates, nonlinear normalization models have been previously used to handle light-induced changes in pupil size [22, 28] (see Section 3). Normalization is the process by which the annular iris region is converted to a rectangular entity via a geometric transformation scheme. *This research investigates the use of nonlinear iris normalization to handle drug-induced pupil dilation.* Since the nonlinear deformation of the iris tissue due to pupil dilation results in changes on the visible features of the stroma (see Figure 2), feature extraction approaches based on key points may be more robust. *In this research, a key point based method proposed by Ma et al. [14] is used for iris matching.*

1.2. Motivation and contribution

While *light-induced* pupil dilation has been extensively investigated, not much work has been done on analyzing and counteracting the effect of *drug-induced* pupil dilation. This work focuses on pupil dilation induced by the use of drugs such as mydriatic agents. Mydriasis or drug-induced pupil dilation has been shown to negatively affect iris recognition performance [7, 21], but no solution has been investigated to counteract its effect on iris recognition. Note that mydriatic agents may be used by an adversary to mask their identity from an iris recognition system. These agents can be easily obtained online without a medical prescription. Hence, there is a need to understand and counteract the effect of such drugs on iris recognition.

The contributions of this work are:

(1) Investigate the impact of drug-induced pupil dilation on iris recognition performance.

(2) Mitigate the effect of drug-induced pupil dilation on iris recognition performance by using (a) nonlinear normalization and (b) key point-based feature extraction.

(3) Investigate any differences between drug- and light-induced pupil dilation from a biological perspective that may lead to differential impact on iris recognition performance.

2. Drug-induced pupil dilation

Pupil size can be deliberately enlarged by using mydriatic agents administered topically or systemically. 1% tropicamide and 2.5% phenylephrine are typically used mydriatic drugs that have different impact on the iris muscles. Tropicamide blocks the parasympathetic nervous system and paralyzes the contraction of the sphincter muscle. This unmasks the effect of the sympathetic nervous system on the dilator muscle. On the other hand, phenylephrine acts directly on the sympathetic nerve receptors located on the dilator muscle. Park *et al*. [16] reported that 1% tropicamide is more effective at inducing pupil dilation than 2.5% phenylephrine.

Tomeo-Reyes and Chandran [21] explored the impact of drug-induced pupil dilation on iris recognition performance, but only from the *template* standpoint. They performed a bit error analysis on the iris code to investigate the effect of light- and drug-induced pupil dilation on the consistency of texture information within the iris and reported an over 10% increase in bit error when matching regular images with dilated images. Dhir *et al*. [7] also reported increased error rates after instillation of a mydriatic agent. They noted that non-elastic deformation in the iris structure occurs after application of dilation drops, resulting in non-circular pupillary boundaries. Circle-based iris localization methods, they state, are therefore inadequate.

3. Nonlinear iris normalization

One of the key stages in classical iris recognition systems is the normalization stage, where the annular segmented iris region is mapped to a fixed-size rectangular structure which can be used to compensate for differences in scale and variations in pupil size. The most commonly used normalization scheme in the literature is Daugman's rubber sheet model [6]. This method adopts linear sampling in the radial and angular directions of the annular iris. However, classical *linear* normalization schemes are only suitable for small variations in pupil size, and are not suitable when the dilation level of the iris images to be matched is very different. Given the nonlinear nature of iris dynamics, *nonlinear* normalization schemes are expected to work better.[1]

Several studies have focused on mathematically modeling the effects of iris deformation due to changes in pupil size. In [27], Wyatt presented the 'minimum-wear-and-tear' meshwork, which models the iris collagen structure as a set of fibers arranged in parallel arcs connecting the limbus and the pupillary boundary in clockwise and counterclockwise directions. Iris deformation is calculated as the addition of linear and nonlinear stretches of such iris fibers. Computer tracking techniques using Elastic Graph Matching (EGM) were used by Phang [17] to analyze iris deformation. His results indicate that movements of the iris surface occur mainly in the radial direction, and that the stretching of the iris surface is nonlinear. Clark *et al*. [4] used biomechanical differential equations to develop a theoretical model for characterizing the nonlinear dynamics of iris deformation. Unlike previous models [17, 27], the biomechanical model proposed in [4] takes into account the elastic properties of the iris and the effects of the iris musculature.

In the nonlinear normalization scheme proposed by Yuan and Shi [28], iris patterns are deformed nonlinearly to conform to a reference annular zone with a fixed dilation ratio $\lambda_{ref} = R_{p_{ref}}/R_s$, where $R_{p_{ref}}$ is the mean pupil radius of all iris images in a database, and R_s is the iris radius. This annular zone is then linearly sampled and converted to a rectangular block of fixed dimensions. The nonlinear deformation model uses virtual arcs subtending an angle of $\pi/2$, which connect points on the pupillary boundary with points on the limbic boundary. These arcs are same as the fibers in Wyatt's model [27]. However, Yuan and Shi's approach is limited since it does not take into account the elastic properties of the iris and muscle activity.

In [22], a biomechanical model based on the work of Clark *et al*. [4] was used to define a nonlinear normalization scheme that improves iris recognition performance in the context of light-induced pupil dilation. The mathematical formulation of the biomechanical model, explained in detail in [4], considers the iris as a thin cylindrical shell in which the z dimension is much smaller than the r and θ dimensions. The iris is viewed as a thin plate where loads are applied uniformly over the z dimension. From an iris recognition standpoint, only the 2D information in the $r-\theta$ plane is considered. Since the iris muscles are distributed throughout the annular region, an axisymmetric load is assumed, and as a result, the displacement u is independent of θ. The displacement $u(r)$ of the iris tissue within the annular region $r \in (r_1, r_2)$ is calculated using the following nonlinear differential equation:

$$u'' + \frac{u'}{r} - \frac{\zeta u}{r^2} - \frac{1-\nu\zeta}{2r}\left(u'\right)^2 - \frac{(\nu-1)\zeta}{2r}\left(\frac{u}{r}\right)^2 - \frac{1}{2}\frac{d}{dr}\left(u'\right)^2 - \frac{\nu\zeta}{2}\frac{d}{dr}\left(\frac{u}{r}\right)^2 = 0, \tag{1}$$

with boundary conditions:

$$u\left(r_1\right) = \mu_1, \mu_1 > 0 \text{ and } u\left(r_2\right) = 0, \tag{2}$$

where $u = u(r)$ is the radial displacement, $()'$ denote ordinary differentiation with respect to r, ν is the Poisson's ratio in the radial direction (i.e., negative ratio of transverse to axial strain of the material), and ζ is the ratio between the Young's moduli in the angular and radial directions (E_θ and E_r) used to measure the level of stiffness of an elastic material. The values $\nu = 0.49$, $E_\theta = 2.97$ kPa and $E_r = 4$ kPa were used in [22] to perform experiments.

[1] Segmentation methods like those proposed by Krichen [13] may also help compensate for the inadequacies of linear normalization schemes.

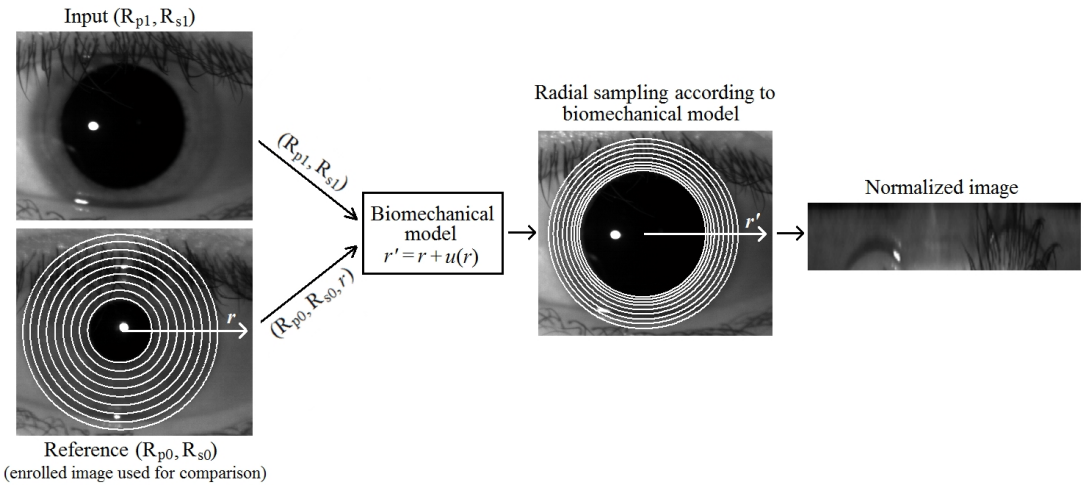

Figure 3: Iris normalization according to the biomechanical model [22]. R_p and R_s are, respectively, the pupil and iris radii, r is a vector of *uniformly* spaced radial positions calculated from the reference image, and r' is a vector of *non-uniformly* spaced radial positions calculated from the nonlinear displacement $u(r)$ estimated by the biomechanical model.

Unlike the rubber sheet model, in which the iris is linearly sampled in the radial direction at each angular position, the nonlinear normalization method presented in [22] that is employed in this work uses nonlinear sampling in the radial direction based on the aforementioned biomechanical model. The process is shown in Figure 3. As observed in the figure, a vector r consisting of uniformly spaced radial positions is first obtained from a reference image, which is the enrolled image (i.e., template). Vector r' is then calculated as $r' = r + u(r)$, where $u(r)$ is the radial displacement estimated by the biomechanical model. The values of r' are used to transform the iris image I from Cartesian to Pseudo-polar coordinates by inversely mapping each location (r', θ) in the transformed image to the location $O(r', \theta)$ in the original image, I. $O(r', \theta)$ is calculated according to equation (3), where P and L represent the points in the pupillary and limbic boundaries, respectively, resulting from the segmentation stage.

$$O(r', \theta) = (1 - r')P(\theta) + r'L(\theta). \quad (3)$$

4. Experimental setup

4.1. Data and data collection protocol

Experiments are carried out using the Iris Degradations Data Set (IDDS). IDDS consists of 2183 iris images acquired at a resolution of 640×480 pixels. Images were taken from 59 participants who provided images of both eyes. The total number of iris classes is thus 118. The sensor used for data collection was the IG-AD100, a dual eye camera which works in the near infrared (NIR) wavelength. IDDS is divided into four subsets: (i) images captured under normal conditions, (ii) images affected by quality degradation due to local noise (gaze deviation, glasses and eyelid obstruction), (iii) images affected by light- and drug-induced pupil dilation and constriction, and (iv) images affected by occlusion. In this work, only the images acquired under normal conditions and those affected by pupil dilation are used. In order to quantify pupil dilation, the ratio between the pupil and iris radii is used. This ratio, denoted as ρ, is referred to as dilation ratio ($\rho = R_{pupil}/R_{iris}$). Sample images with different dilation ratios are shown in Figure 4.

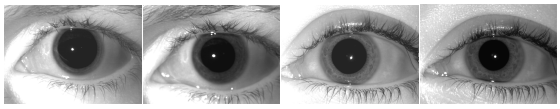

(a) (b) (c) (d)

Figure 4: Sample images affected by various degrees of pupil dilation. Samples are affected by drug-induced dilation ((a) $\rho = 0.75$ and (b) $\rho = 0.59$)), and light-induced dilation ((c) $\rho = 0.58$ and (d) $\rho = 0.52$)).

- *Normal conditions (IDDS:NC)*: This subset includes a total of 354 iris images captured under normal room illumination in a controlled environment. Images were taken from the 59 different participants who provided 3 images per eye.
- *Light-induced pupil dilation (IDDS:Dilation-light)*: This subset comprises 112 iris images from 32 different eyes. Images from this subset were obtained by turning off the ambient lighting. The infrared LEDs used by the IG-AD100 to illuminate the iris were enough to take high-quality iris images in the absence of ambient light. The ratio between the pupil and iris radii, or dilation ratio, varies from 0.515 to 0.625 for irides in this subset.
- *Drug-induced pupil dilation (IDDS:Dilation-drugs)*: This subset includes 415 iris images from 19 different eyes. A mydriatic agent (1% tropicamide) in the form of eye drops was instilled in participants. Irides in this subset show dilation ratios in the range 0.515 to 0.755.

  The following protocol was used for data collection (IRB approved):

1. Provide signed consent for administration of eye drops by a registered optometrist.
2. Provide demographic information (age, gender and ethnicity).
3. Complete screening questions regarding:
   - previous diagnosis of glaucoma,
   - history of glaucoma in the family/blood relatives,
   - ocular surgeries,
   - previous instillation of mydriatic agents and abnormal reactions to it (if any),
   - previous diagnosis of high blood pressure, heart disease, diabetes, over-active thyroid, asthma, retinal detachment and high myopia, and
   - list of drugs prescribed by the doctor and bought from the pharmacist taken within the last month.
4. Pre-test check up by the optometrist, including:
   - Intraocular pressure. Exclude subject if > 21 mm Hg.
   - Ophthalmoscopy measurements of cup/disc (C/D) ratio. Exclude if glaucomatous signs or posterior subcapsular cataract are detected.
   - Van Herrick test (gap/cornea). Exclude subject if < 0.3.
5. Instillation of one drop of tropicamide 1% in left eye. Right eye was used if recommended by the optometrist. After the drug was applied, images were taken every 3-5 minutes, but considerable time elapsed before full dilation occurred (20-30 minutes).
6. Post-test check up by the optometrist and debriefing. Following the instillation of tropicamide, the pupil can remain dilated for 5 to 6 hours.

According to the protocol, participants could be excluded from data collection based on their health record. Although no participant was rejected, it is important to note that there might be a subset of the population who may never use this drug given the risk involved in instilling it.

4.2. Iris recognition system

The iris recognition software used in the experiments is USIT v2.1.0 (University of Salzburg Iris Toolkit v2.1.0), a publicly available software package [18] which comprises different algorithms for iris pre-processing, feature extraction, and comparison.

Segmentation is performed in this work using the USIT implementation of two different methods:

– *Circular boundaries*: Contrast-adjusted Hough transform is used to calculate circular boundaries. Contrast adjustment is used to enhance the iris boundaries and Canny edge detection is performed.

– *Elliptical boundaries*: Weighted adaptive Hough and ellipsopolar transforms [24] are used to calculate elliptical boundaries. First, a region of interest (ROI) is iteratively refined to find a center point. The boundaries are then extracted from an ellipsopolar representation of the iris.

Once the iris boundaries are located, masks are created manually to eliminate those pixels corresponding to eyelids, eyelashes and reflections. Only minor imperfections that cannot be manually eliminated remain.

In the *normalization stage*, the iris image is remapped from Cartesian to Pseudo-polar coordinates. In the case of the rubber sheet model [6], a vector r of uniformly spaced *radial* positions in the interval $[0, 1]$ is used. When the biomechanical model is used, the vector r is replaced with $r' = r + u(r)$ as explained in Section 3. The resulting normalized images have a size of 512×64. P and L are modeled as circles or ellipses depending upon the segmentation method used (see equation (3)).

Two different *feature extraction* methods are used (see Figure 5): log-Gabor feature extraction, which calculates the phase response *at each pixel* (dense sampling approach), and Ma *et al*.'s algorithm, which uses *local sharp variation points* (sparse sampling approach). In both cases, normalized iris images are divided into 10 1-D intensity signals, each one averaged from the pixels of 5 adjacent rows.

– *1-D log-Gabor feature extraction* (re-implementation of Masek's algorithm [15]): In this algorithm, the 10 1-D intensity signals are convolved with a 1-D log-Gabor filter. The phase response *at each pixel* specifies the coordinates of a phasor in the complex plane. During phase encoding, the angle of each phasor is quantised to one of the four quadrants, setting 2 bits of phase information.

– *Algorithm of Ma et al*. [14] (re-implementation): A quadratic spline wavelet transform is first applied to the 10 1-D signals in this algorithm. The maxima and minima (*local sharp variation points*) of the transform from two specific sub-bands are found, and the distance between adjacent maxima and minima is encoded along with a sign that indicates the transition from maximum to minimum or vice versa. This distance denotes the angular separation between key local variation points.

In the *comparison or matching stage*, for both feature extraction methods, the dissimilarity between feature vectors

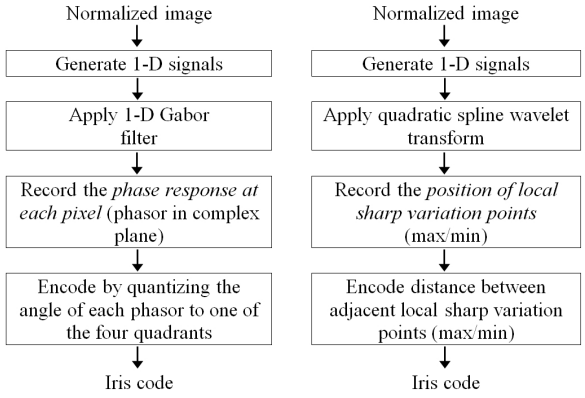

Figure 5: Feature extraction using USIT v2.1.0. Log-Gabor [15] (left) and Ma *et al*. [14] (right).

is computed using the Hamming distance. Rotation invariance is obtained by comparing different shifts of the sample feature vector with the template, and choosing the shift (in the range -8 to 8) that yields the smallest Hamming distance.

5. Experimental results

In this section, the impact of drug-induced pupil dilation on iris recognition performance is first quantified. Then, the efficacy of biomechanical-based nonlinear normalization [22] and key point-based feature extraction [14] to counteract performance degradation is analyzed. Finally, the impact of drug- and light-induced pupil dilation on iris recognition performance is compared and related to the anatomical effects that occur in both cases.

Based on our observation (and also in [7]) that the non-elastic deformation of the iris tissue due to application of dilation drops may result in non-circular pupillary boundaries, the circle- and ellipse-based segmentation methods were compared in this work (see Section 4.2). As expected, better results were obtained when using elliptical segmentation, so this is the method used in all experiments reported in this section. To compute the dilation ratio ($\rho = R_{pupil}/R_{iris}$) and apply the biomechanical model, the pupil and iris radii are calculated by using approximated circles that have the same area as the corresponding ellipses. The radius R of each circle is calculated as $R = \sqrt{a * b/4}$, where a and b, respectively, are the major and minor axes of the ellipse. Images from the IDDS subsets used in this paper are automatically segmented and then subjected to a visual selection process to retain only those that are correctly segmented. Details about the resulting subsets can be found in Table 2.

Table 2: Database information.

Database	**Dilation ratio** $\rho = R_{pupil}/R_{iris}$	**Iris classes**	**Total images**	**Images used**
IDDS:NC	$0.265 < \rho < 0.515$	118	354	245
IDDS:Dilation-light	$0.515 \leq \rho < 0.625$	32	112	100
IDDS:Dilation-drugs	$0.515 \leq \rho < 0.755$	19	415	345

5.1. Effect of drug-induced pupil dilation

The impact of drug-induced pupil dilation on iris recognition performance is evaluated by matching dilated iris samples from *IDDS:Dilation-drugs* with iris templates having a normal dilation ratio. This result is compared with the case where images having a normal dilation ratio from *IDDS:NC* are matched with iris templates also exhibiting a normal dilation ratio. Note that the range of the dilation ratio under normal illumination conditions is between 0.265 and 0.515 (see Table 2). In all cases, the iris images are normalized using the rubber sheet model implemented in USIT. The result is shown in Figure 6. According to the figure, *the non-elastic deformation of the iris tissue after application of a mydriatic agent degrades iris recognition performance.*

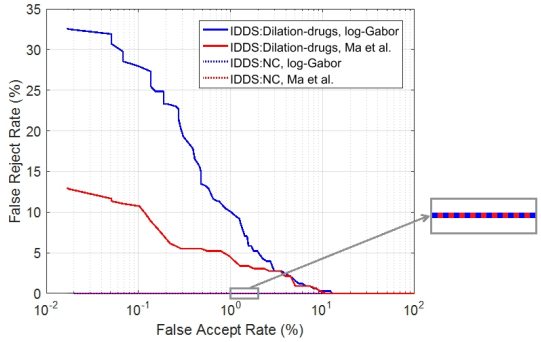

Figure 6: Iris recognition error rates on *IDDS:Dilation-drugs* and *IDDS:NC*. Iris samples from both subsets are matched with iris templates having a normal dilation ratio ($0.265 < \rho < 0.515$). Rubber sheet model is used for normalization. Note that error rates for IDDS:NC are 0 regardless of the feature extraction method.

5.2. Analysis of nonlinear normalization and key point based features

This section analyzes the efficacy of biomechanical model-based nonlinear normalization [22] and key point-based feature matching (Ma *et al.*'s algorithm [14]) to counteract the performance degradation arising from drug-induced pupil dilation. The performance of the selected normalization scheme is evaluated on *IDDS:Dilation-drugs* and compared to that of the rubber sheet model. Results are shown in Figure 7. Error rates (FRR@FAR=0.02% and FRR@FAR=1%) are summarized in Table 3. It must be noted that there is a limit to the degree of useful iris information that can be gleaned in cases of extreme dilation due to the implicit band limit of the radial iris signal. Thus, the proposed approach can breakdown in the extreme case.

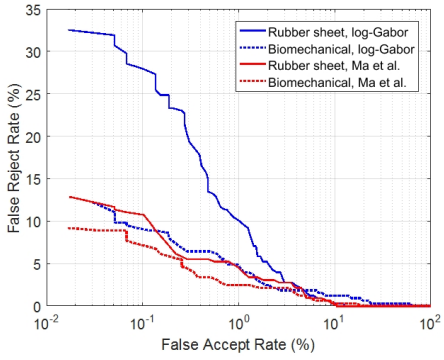

Figure 7: Iris recognition error rates on *IDDS:Dilation-drugs*. Iris samples from this subset are matched with iris templates having a normal dilation ratio ($0.265 < \rho < 0.515$).

Table 3: Error rates obtained for *IDDS:Dilation-drugs* using log-Gabor features and Ma *et al.*'s (key point based) features.

Method	**FRR@FAR=0.02% (%)**		**FRR@FAR=1% (%)**	
	Rubber	**Biomechanical**	**Rubber**	**Biomechanical**
Log-Gabor	32.76	12.57	10.10	4.72
Ma *et al.*	13.15	9.21	4.48	2.45

According to the results, the biomechanical approach to iris normalization results in better performance than the rubber sheet model. The improvement is more noticeable when using log-Gabor based feature extraction, with values of the FRR@FAR=1% decreasing by a factor of 2.72. A reduction by a factor of 1.82 can be observed when using Ma *et al.*'s algorithm. *Considerably lower error rates are obtained when using Ma et al. 's algorithm for two main reasons. First of all, pupil dilation is mainly a radial effect, and it only mildly affects the angular separation between key points (used by Ma et al. for encoding).* The intensity variations across the sampled points in the normalized image, however, might be quite significant and therefore the log-Gabor quantized phase features are more severely affected. *Secondly, it is also possible that features appear or disappear because of the radial displacement caused by pupil dilation. Ma's algorithm provides some robustness to this because there is averaging in the vertical (radial) direction. The wavelet transform scale ensures that features are extracted based on blocks rather than individual sample points, and a threshold is used in their algorithm to suppress faint local variations that are unreliable.*

5.3. Light- vs drug-induced pupil dilation

The impact of drug- and light-induced pupil dilation on iris recognition performance is compared in this section (see sample images in Figure 4). In all cases, the feature vectors are obtained using the USIT implementation of Ma *et al.* (key point based algorithm). Results are shown in Figure 8.

According to the results, the impact of drug-induced pupil dilation is more severe than that of light-induced pupil dilation. One of the reasons for this is that the dilation ratio of the images in *IDDS:Dilation-drugs* is higher than that of the images in *IDDS:Dilation-light*. While the maximum dilation ratio in *IDDS:Dilation-drugs* reaches 0.755, it only reaches 0.625 in *IDDS:Dilation-light*. *This fact indicates that higher dilation ratios can be more easily achieved when using drugs.* To verify that any change in performance is primarily due to the use of light or drugs, an experiment was conducted in which *IDDS:Dilation-drugs* was trimmed to only include images with a maximum dilation ratio equal to 0.625 as in the case of light-induced dilation. Even in this reduced dataset, the error rates were observed to be worse in the case of drug-induced dilation.

The fact that drug-induced pupil dilation results in poorer error rates than light-induced might be explained by the fact that the mydriatic agent (1% tropicamide) acts by unmasking the effect of the sympathetic nervous system on the dilator muscle after paralyzing the sphincter muscle, and so its effect on the iris structure could be more severe than the effect provoked by the absence of light. In both cases, however, the biomechanical normalization model resulted in better performance than the rubber sheet model.

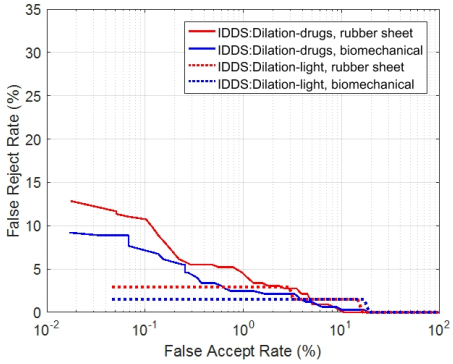

Figure 8: Iris recognition error rates on *IDDS:Dilation-drugs* and *IDDS:Dilation-light*. Iris samples from both subsets are matched with iris templates having a normal dilation ratio ($0.265 < \rho < 0.515$). Ma *et al.*'s feature extraction algorithm is used.

5.4. Observations

The observations linked to the three main contributions of this work can be summarized as follows:

(1) According to the ophthalmological literature, the mydriatic agent tropicamide blocks the parasympathetic nervous system and paralyzes the contraction of the sphincter muscle. This unmasks the effect of the sympathetic nervous system on the dilator muscle. This effect causes a non-elastic deformation of the iris tissue that severely degrades iris recognition performance. Such a deformation also results in non-circular pupillary boundaries and, therefore, iris localization methods like those based on ellipses are more appropriate.

(2) When matching iris samples affected by drug-induced dilation against samples exhibiting normal dilation ratio, biomechanical model-based nonlinear normalization results in better performance than linear normalization schemes like the classical rubber sheet model. Since the nonlinear deformation of the iris tissue due to pupil dilation results in localized changes on the visible features of the stroma and occurs mainly in the radial direction, feature extraction approaches based on angular separation between key points, as the one proposed by Ma *et al.*, result in better performance.

(3) The effect of light-induced pupil dilation is not as severe as that of drug-induced. This result might be explained by the fact that mydriatic agents paralyze the iris muscles, so their effect on the iris structure is more severe than the effect provoked by the absence of light.

6. Conclusions

Mydriasis or drug-induced pupil dilation has been shown to negatively affect iris recognition performance. Since it increases the chances of a false non-match, it can potentially be used by an adversary to mask their identity via obfuscation. In this work, details of the effect of mydriatic

drugs on pupil dilation were provided, along with a protocol to collect iris images affected by drug-induced dilation. In addition, it was demonstrated that a nonlinear normalization scheme followed by key point based feature encoding may be more suitable for matching irides with large differences in pupil size. The FRR@FAR=1% obtained with the biomechanical model on the *IDDS:Dilation-drugs* database is better by 2.03% (a factor of 1.82) compared to the classical rubber sheet model when using Ma *et al*.'s key point based feature extraction method. Drug-induced pupil dilation was also shown to result in higher iris recognition error rates than light-induced pupil dilation.

Acknowledgments

The authors are grateful to Prof. David Atchison for his assistance with the data collection activity.

References

[1] Chinese Academy of Sciences, Institute of Automation: Biometrics Ideal Test. URL: http://biometrics.idealtest.org.

[2] S. S. Arora, M. Vatsa, R. Singh, and A. Jain. Iris recognition under alcohol influence: A preliminary study. In *International Conference on Biometrics*, pages 336–341, 2012.

[3] O. Bergamin, M. B. Zimmerman, and R. H. Kardon. Pupil light reflex in normal and diseased eyes: Diagnosis of visual dysfunction using waveform partitioning. *Ophthalmology*, 110(1):106 – 114, 2003.

[4] A. D. Clark, S. A. Kulp, I. H. Herron, and A. Ross. A theoretical model for describing iris dynamics. In *Handbook of Iris Recognition*, pages 129–150. Springer, 2013.

[5] S. G. Crihalmeanu and A. Ross. Pupil light reflex in the context of iris recognition – Data acquisition setup. Technical report, West Virginia University, 2014.

[6] J. G. Daugman. High confidence visual recognition of persons by a test of statistical independence. *IEEE Transactions on Pattern Analysis and Machine Intelligence*, 15(11):1148–1161, 1993.

[7] L. Dhir, N. E. Habib, D. M. Monro, and S. Rakshit. Effect of cataract surgery and pupil dilation on iris pattern recognition for personal authentication. *Eye*, 224(6):1006–1010, 2010.

[8] S. P. Fenker and K. W. Bowyer. Analysis of template aging in iris biometrics. In *IEEE Computer Society Conference on Computer Vision and Pattern Recognition Workshops*, pages 45–51, 2012.

[9] S. D. Goldinger and M. H. Papesh. Pupil dilation reflects the creation and retrieval of memories. *Current Directions in Psychological Science*, 21(2):90–95, 2012.

[10] P. J. Grother, J. R. Matey, E. Tabassi, G. W. Quinn, and M. Chumakov. IREX VI - Temporal stability of iris recognition accuracy. Technical report, NIST, 2013.

[11] E. H. Hess and J. M. Polt. Pupil size in relation to mental activity during simple problem-solving. *Science*, 143(3611):1190–1192, 1964.

[12] K. Hollingsworth, K. W. Bowyer, and P. W. Flynn. Pupil dilation degrades iris biometric performance. *Computer Vision and Image Understanding*, 113(1):150–157, 2009.

[13] E. Krichen. Lef3a: Pupil segmentation using Viterbi search algorithm. In *International Conference on Biometrics*, pages 323–329, 2012.

[14] L. Ma, T. Tan, Y. Wang, and D. Zhang. Efficient iris recognition by characterizing key local variations. *IEEE Transactions on Image Processing*, 13(6):739–750, 2004.

[15] L. Masek. Recognition of human iris patterns for biometric identification. Master's thesis, University of Western Australia, 2003.

[16] J. H. Park, Y. C. Lee, and S. Y. Lee. The comparison of mydriatic effect between two drugs of different mechanism. *Korean Journal of Ophthalmology*, 23(1):40–42, 2009.

[17] S. S. Phang. Investigating and developing a model for iris changes under varied lighting conditions. Master's thesis, Queensland University of Technology, 2007.

[18] C. Rathgeb, A. Uhl, and P. Wild. *Iris recognition: From segmentation to template security*. Advances in Information Security. Springer, 2012.

[19] O. Seyeddain, H. Kraker, A. Redlberger, A. K. Dexl, G. Grabner, and M. Emesz. Reliability of automatic biometric iris recognition after phacoemulsification or drug-induced pupil dilation. *European Journal of Ophthalmology*, 24(1):58–62, 2014.

[20] J. Thornton, M. Savvides, and B. V. K. Vijaya Kumar. A Bayesian approach to deformed pattern matching of iris images. *IEEE Transactions on Pattern Analysis and Machine Intelligence*, 29:596–606, 2007.

[21] I. Tomeo-Reyes and V. Chandran. Effect of pupil dilation and constriction on the distribution of bit errors within the iris. In *IEEE International Conference on Computer Vision and Pattern Recognition Workshops*, 2014.

[22] I. Tomeo-Reyes, A. Ross, A. D. Clark, and V. Chandran. A biomechanical approach to iris normalization. In *International Conference on Biometrics*, pages 9–16, 2015.

[23] R. S. Tubbs, E. Rizk, M. M. Shoja, M. Loukas, N. Barbaro, and S. R. J., editors. *Nerves and Nerve Injuries: Vol 1: History, Embryology, Anatomy, Imaging and Diagnostics*. Academic Press, Elsevier, 2015.

[24] A. Uhl and P. Wild. Weighted adaptive hough and ellipsopolar transforms for real-time iris segmentation. In *International Conference on Biometrics*, pages 283–290, 2012.

[25] Z. Wei, T. Tan, and Z. Sun. Nonlinear iris deformation correction based on gaussian model. In S. W. Lee and S. Z. Li, editors, *Advances in Biometrics*, volume 4642 of *Lecture Notes in Computer Science*, pages 780–789. Springer, 2007.

[26] B. Winn, D. Whitaker, D. B. Elliott, and N. J. Phillips. Factors affecting light-adapted pupil size in normal human subjects. *Investigative Ophthalmology & Visual Science*, 35(3):1132–1137, 1994.

[27] H. J. Wyatt. A 'minimum-wear-and-tear' meshwork for the iris. *Vision Research*, 40:2167–2176, 2000.

[28] X. Yuan and P. Shi. A non-linear normalization model for iris recognition. In *Advances in Biometric Person Authentication*, volume 3781 of *Lecture Notes in Computer Science*. Springer, 2005.